Measuring Cerebral Activation from fNIRS Signals: an Approach Based on Compressive Sensing and Taylor-Fourier Model

Guglielmo Frigo, Sabrina Brigadoi, Giada Giorgi, Giovanni Sparacino, and Claudio Narduzzi

Abstract—Functional near-infrared spectroscopy (fNIRS) is a non-invasive and portable neuroimaging technique that uses near-infrared light to monitor cerebral activity by the so-called haemodynamic responses (HRs). The measurement is challenging because of the presence of severe physiological noise, such as respiratory and vasomotor waves. In the present paper, a novel technique for fNIRS signal de-noising and HR estimation is described. The method relies on a joint application of Compressed Sensing theory principles and Taylor-Fourier modelling of non-stationary spectral components. It operates in the frequency domain and models physiological noise as a linear combination of sinusoidal tones, characterized in terms of frequency, amplitude and initial phase. Algorithm performance is assessed over both synthetic and experimental data-sets, and compared with that of two reference techniques from fNIRS literature.

Keywords—*functional near-infrared spectroscopy; haemodynamic response; physiological noise; short-separation channels; denoising; compressive sensing; Taylor-Fourier modelling*

I. INTRODUCTION

Near-infrared (NIR) spectroscopy is widely employed for sensing and measurement e.g. in [1]–[4]. A variety of medical measurement applications, ranging from the monitoring of blood oxygenation level [5] to detection of circulatory diseases (e.g. an arterial or venous occlusion) and glucose sensing [6], [7], also rely on this technique.

In neuroscience, functional near-infrared spectroscopy (fNIRS) is used to monitor cerebral activity and study healthy or pathological brain activation to a variety of cognitive tasks [8]. Since, after a particular stimulus or during a task, changes occur in the concentrations of oxy-(HbO) and deoxy-(HbR) haemoglobin (i.e., the molecules carrying oxygen in the blood), these concentration changes can be interpreted as indirect measurements of neural activity in the investigated brain area. fNIRS operates in the red and near-infrared wavelength range (650 to 950 nm), where HbO and HbR are the main absorbers of light while other biological tissues such as skin and skull are mainly transparent [9]. HbO and HbR concentration changes can thus be recovered from fNIRS signals, yielding what is called the *haemodynamic response* (HR) [10].

Accurate fNIRS-based estimation of HR is, however, extremely difficult. Light in the near-infrared range, emitted by sources placed on the subject's head, reaches the cortex and is back-scattered to detectors positioned several centimeters from the source, hence travelling through the scalp, skull and cerebrospinal fluid twice. Since the human scalp and skull are highly vascularized, fNIRS signals are strongly affected by cardiac activity, respiration and vasomotion, which are in fact predominant. As a result, within the expected bandwidth, HR is buried in 'physiological' noise that needs to be removed to recover true brain activity. Furthermore, changes in heart rate and pressure of a subject may be correlated to a task, as common emotional responses [11], introducing the possibility of time-correlated disturbances.

A well known de-noising technique consists in accurately estimating the noise signal first, then subtracting it from the acquired signal in order to clean it up. This technique is widely used in many contexts, ranging from speech recognition to biomedical applications where signal-to-noise ratios (SNRs) can be dramatically low [12], [13]. De-noising gets more difficult when physiological noise disturbances are non-stationary, as in the fNIRS case, since both their amplitude and spectral support can vary according to unpredictable and uncorrelated trends.

In this context, the most challenging aspect is the accurate measurement of the noise template that will then be subtracted from the acquired waveform. The problem has been approached in some cases by subtracting an average noise estimate obtained over a number of signal segments [14]. However, results may not be entirely satisfactory as the variable part of the disturbance, which is left untouched, can still be significant.

This paper proposes a novel processing approach for reliable de-noising of fNIRS signals and improved HR estimation. A super-resolution technique, based on Compressive Sensing (CS) theory, is employed to estimate the spectral support of the noise signal over a reasonably short observation interval [15]. Then, parameters of a Taylor-Fourier multifrequency (TFM) model of the signal are identified, taking into account Taylor expansion terms up to the second order to accurately estimate also the amplitudes of noise components. A similar approach has already been used with good results for gradient artifact removal in concurrent electro-encephalographic and magnetic resonance imaging acquisitions [16].

This work extends a study presented in preliminary form in [17] and is organized as follows. In Section II the state

G. Frigo, G. Giorgi, C. Narduzzi and G. Sparacino are with the Department of Information Engineering of the University of Padova, Via Gradenigo 6/b, 35131 Padova, Italy (e-mail: {frigogug, giada, narduzzi, gianni}@dei.unipd.it).

S. Brigadoi is with the Department of Developmental Psychology of the University of Padova, Via Venezia 8, 35131 Padova, Italy (email: sabrina.brigadoi@unipd.it).

of the art in HR retrieval techniques is briefly discussed. In Section III the proposed algorithm is thoroughly described, focusing the attention particularly on CS and TFM stages. To assess the algorithm both synthetic and real experimental data, illustrated in Section IV, are employed. Finally, in Section V algorithm performance in terms of denoising capabilities and HR recovery accuracy are assessed, also by a comparison with two reference techniques from the fNIRS literature.

II. STATE OF THE ART

fNIRS is widely used as a non-invasive and portable neuroimaging technique. Recovering the informative part of the desired HR signal from fNIRS measurements affected by physiological noise is very challenging [18], [19] because, for example, fluctuations arising from vasomotor waves have a frequency content (~0.04-0.15 Hz) that is superposed on the expected HR bandwidth. Furthermore, physiological fluctuations usually have higher amplitude than HR.

Several techniques have been proposed over the years. A very simple and frequently used one is Conventional Averaging (CA). The measured signal is simply band-pass filtered (0.01 – 3 Hz) to reduce high frequency noise and very slow trends, then segmented into trials, each referred to a single kind of stimulus. Trials related to the same stimulus type are averaged together to obtain a mean HR. This is further smoothed with a Savitzky-Golay filter with polynomial order equal to 3 and frame size equal to 25 time-points. CA relies on working hypotheses that may be questionable in practice, namely, exact statistical independence between HR and physiological noise components, as well as a difference in phase between stimulus presentation rate and physiological oscillations, ensuring mutual uncorrelation. As a result, the number of trials necessary to accurately recover the underlying HR might be very large, thus influencing overall experiment duration. Furthermore, when physiological noise oscillations and stimulus presentation rate are in phase, CA cannot distinguish between the two contributions.

Given the proportionality between source-detector distance and depth sensitivity (that is, increasing source-detector distance increases the proportion of photons that travelled to deeper regions of the head [20]), a signal obtained with source-detector distance shorter than 1 cm is expected to reflect only superficial haemodynamic changes, induced by physiological fluctuations but uncorrelated with stimulus-evoked brain activity. The method proposed in [19], [21] assumes that, in parallel to the 'standard' (long-separation – LS) fNIRS signal, containing both HR and noise, a 'background' (short-separation – SS) fNIRS signal is also collected. SS channels are highly sensitive to superficial tissues and ideally should have zero brain sensitivity. Therefore, the signal measured by an SS channel should contain only noise components, which can be subtracted from a simultaneously acquired LS signal for de-noising.

In spite of the proven utility of SS signals, it is often counterproductive to subtract the whole SS signal from the LS one. In fact, only low-frequency physiological components, whose spectral content is similar to HR, should be extrapolated from the SS channels and subtracted from the LS ones. Furthermore, non stationarity implies that physiological contributions may significantly vary in both amplitude and spectral support, even during a single HR event.

The recently proposed Reference-channel Modelling Corrected Bayesian Approach (ReMCoBA) [22], [23] is a two-step method. First, a model of physiological noise is derived from the SS signal and subtracted from the LS signal. Then, corrected LS data are further filtered, on a single trial basis, by a non-parametric Bayesian approach, in order to reduce residual random noise. ReMCoBA is able to estimate low-frequency physiological components of interest from the SS signal using a parametric multi-sine model. It is a model-free method for HR recovery, since no prior information is required about the underlying HR and recovery has been shown to be accurate both in a synthetic and a real experimental scenario. However, estimation of physiological noise model parameters is not always easy and sometimes fails, since the frequency spectrum is computed on a limited number of samples.

In Section V, ReMCoBA and CA are taken as reference methods for comparison.

III. PROPOSED METHOD

The method proposed in this paper assumes that both LS and SS signals are acquired by fNIRS. In the time domain, sequences are defined over the discrete set of integer multiples of the sampling period $T_s = 1/F_s$.

A. Measurement data model

From a mathematical viewpoint, data can be described by a superposition of haemodynamic response $r[n]$, physiological noise $n_P[n]$ and measurement uncertainty $n_M[n]$:

$$\begin{align} x_{LS}[n] &= r[n] + n_P[n] + n_M[n] \\ x_{SS}[n] &= n_P[n] + n_M[n]. \end{align} \tag{1}$$

The contribution of HR is only present in LS channels.

The random process $n_M[n]$, which accounts for any source of uncertainty related to the acquisition stage, particularly ADC quantization error and non-ideal detector resolution, is represented by white Gaussian noise.

A multisine model is adopted for physiological noise $n_P[n]$, in the form:

$$n_P[n] = \sum_{i=1}^{5} A_i \sin\left(2\pi f_i n T_s + \phi_i\right), \tag{2}$$

where amplitudes and frequencies of the 5 components, simulating heart beat, respiration, vasomotion, slow and very slow physiological trends, vary randomly to simulate differences among channels and non-stationarity of physiological oscillations in the same channel.

The aim of the CS-TFM algorithm is to accurately identify the parameters of the physiological noise template (2) from the SS channel, then subtract the resulting estimate $\hat{n}_P[n]$ from the standard channel. For each considered LS and SS channel
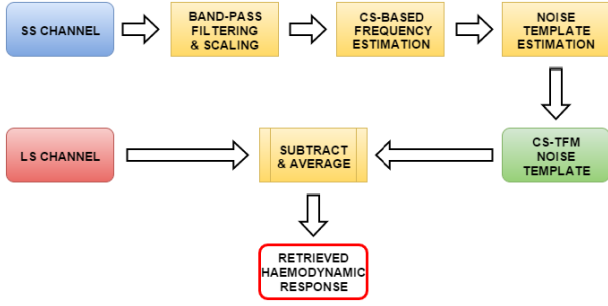
Fig. 1. Block diagram of the proposed algorithm main steps.

pair, a specific noise template is computed and the de-noised single-trial HR profile:

$$\hat{r}[n] = x_{LS}[n] - \hat{n}_P[n] \qquad (3)$$

is obtained. This signal is then segmented into estimated HRs, that are grouped according to the stimulus type and averaged to obtain, for each subject and channel, the mean HR in each condition.

A block diagram summarizing the steps involved in the proposed algorithm is reported in Fig.1.

B. Band-pass filtering and scaling

In the fNIRS de-noising pipeline, it is common practice to apply a band-pass filter to both LS and SS sequences before any other processing takes place, attenuating any component outside the range $[0.01 \div 0.55]$ Hz. HR spectrum is likely to exhibit a central frequency approximately equal to 0.08 Hz. As the sampling frequency selected for experimental data acquisitions is 7.8125 Hz, the filter normalized bandwidth is approximately 0.07. Therefore, realization by means of a discrete finite impulse response (FIR) filter requires filter order to be at least 50 (Hanning window employed in the synthesis).

fNIRS measurements also need to be suitably coupled and, for each LS channel, the SS channel with the highest correlation is chosen. Furthermore, due to the different paths crossed by photons, LS and SS acquisitions may differ in mean and standard deviation by up to one order of magnitude. Before any further processing, then, the SS sequence has to be suitably scaled according to a least square fitting approach. Data acquired during a resting state period, where no significant HR contribution is expected and it is reasonable to suppose that physiological noise contributions are similar in LS and SS channels, are generally considered for this purpose.

C. CS-based frequency estimation

CS-based super-resolution allows to overcome some of the limitations of traditional DFT-based frequency analysis and obtain accurate frequency estimates while working with shorter observation intervals [15], [24]. For a given size of the data record, it can reduce frequency uncertainty by one order of magnitude over the standard DFT, properly accounting for spectral leakage and long-range interference effects in

truncated DFT series. The super-resolution method is briefly summarized here for the sake of completeness.

Let $x_{SS}[n]$ be divided into consecutive non-overlapping records of N samples. Arranging record data into a column vector $\mathbf{x}$, its DFT coefficients can be expressed by the following linear matrix relationship:

$$\mathbf{y} = \mathbf{W}\mathbf{x} \qquad (4)$$

where $\mathbf{W}$ is a $N \times N$ DFT matrix and complex DFT coefficient values are defined on a frequency grid with step $\Delta f_{DFT} = 1/(NT_s)$, where T_s is the sampling interval in fNIRS measurements.

Vector $\mathbf{y}$ can be modelled as a linear projection on a denser frequency grid with step $\Delta f_{CS} = 1/(HT_s)$, $H \gg N$, by:

$$\mathbf{y} = \mathbf{D}\mathbf{b} \qquad (5)$$

where $\mathbf{D}$ is a projection matrix of size $N \times H$ and $\mathbf{b}$ is a vector of complex Fourier amplitudes. For the sake of simplicity, H is assumed to be an integer multiple of N, namely $H = pN$, where the integer p is called *super-resolution factor* and determines the gain with respect to the standard DFT grid. This means a frequency component f_i could be located to within $\pm \Delta f_{CS}/2$.

Since $\dim(\mathbf{y}) \ll \dim(\mathbf{b})$, equation (5) is under-determined and does not allow a closed-form solution. However (2) shows that, by construction, $n_P[n]$ is *sparse* in the frequency domain. Accordingly, a *small* set of elements in $\mathbf{b}$ is expected to have significantly larger magnitude than others. Their indexes form a set $\mathcal{S}$ called the *signal support* whose cardinality $|\mathcal{S}|$ depends on the number of significant components, hence $|\mathcal{S}| \ll N$.

Following the principles of CS theory, the sparsity assumption is exploited to yield the best estimate of $\mathbf{b}$ as the vector that satisfies the following condition:

$$\hat{\mathbf{b}} = \arg\min_{\mathbf{b}} \parallel \mathbf{b} \parallel_1 \quad s.t. \quad \parallel \mathbf{y} - \mathbf{D}\hat{\mathbf{b}} \parallel_2^2 \leq \varepsilon \qquad (6)$$

where ε depends on the energy associated to non-sinusoidal signal components, namely the random noise component $n_M[n]$. In the fNIRS case, the power ratio between $n_P[n]$ and $n_M[n]$ is expected to be not lower than 10 dB.

The algorithm key point is the recovery of signal support $\mathcal{S}$, that allows to express $\mathbf{y}$ as a linear combination of a selected subset of columns of $\mathbf{D}$, whose indices belong to $\mathcal{S}$. These indices are determined directly from $\mathbf{x}$ via an iterative greedy approach known as Orthogonal Matching Pursuit (OMP) [25]. Search iterations are stopped when the current approximation error satisfies condition (6), no a priori information about the support cardinality being required.

Support $\mathcal{S}$ identifies the frequencies of physiological noise components on the dense grid. Given $h \in \mathcal{S}$, the corresponding frequency estimate is $\hat{f}_h = h \cdot \Delta f_{CS} \pm \Delta f_{CS}/2$. Due to numerical conditioning effects, some performance degradation is apparent as p gets larger, since coherence among the columns of $\mathbf{D}$ is increased as well. Nevertheless, OMP ensures exact solutions with overwhelming probability for SNR≥ 10 dB and $p < 15$ if p and N are coprimes, so that numerical singularity problems are prevented [24].

D. Noise template estimation

Once component frequencies are known, identification of the noise template requires the accurate estimation of component amplitudes. A straightforward approach based on least-squares regression over the set of Fourier kernels:

$$\psi_h[n] = e^{\pm j2\pi \hat{f}_h n T_s}. \tag{7}$$

would neglect dynamic trends related to non-stationary conditions. More precisely, their effect would be averaged over the entire observation interval. To cope with non-stationarity within the data record, the SS signal spectral content is represented by a Taylor-Fourier Multifrequency (TFM) model [16], [26].

A K-th order Taylor expansion of (7) defines the transform kernels:

$$\psi_{(k,h)}[n] = (nT_s)^k e^{\pm j2\pi \hat{f}_h n T_s} \quad k = 0, \dots K, \tag{8}$$

whereby each signal component can be represented by a set of K linearly independent time-modulated kernels. This allows to account for variations in both amplitude and instantaneous phase according to individual complex envelopes.

For each considered SS segment, the TFM model is identified from the data record under investigation. The recovered support $\mathcal{S}$ is exploited to develop a vector basis collected in matrix $\mathbf{B}$:

$$\mathbf{B} = \{\psi_{(k,h)}[n] \ : \ h \in \mathcal{S}, \ k = 0 \dots K\} \tag{9}$$

which spans a subspace $\mathcal{T}$ of the Hilbert space of complex-valued functions $\mathcal{L}_2(\mathbb{R})$. Physiological noise is approximated by a linear expansion over the selected basis functions as:

$$\hat{n}_P[n] = \sum_{k=0}^{K} \sum_{h \in \mathcal{S}} z_{(k,h)} \psi_{(k,h)}[n] \tag{10}$$

TFM coefficients $z_{(k,h)}$ are obtained by least-squares projection on the Taylor-Fourier kernel set as:

$$\mathbf{z} = (\mathbf{B}^H \mathbf{B})^{-1} \mathbf{B}^H \mathbf{x} \tag{11}$$

where superscript H indicates the Hermitian transpose. Vector $\mathbf{z}$ contains the terms of the Taylor expansions of physiological noise components:

$$z_{(k,h)} = \frac{(nT_s)^k}{k!} \frac{d^k A_h(t) e^{jP_h(t)}}{dt^k}. \tag{12}$$

In other words, TFM coefficients account not only for static estimates of amplitude and initial phase, but also for their k-th order time derivatives, referred to the mid-point of the observation interval.

Equation (10) can be considered a detailed model of physiological components, where inherent cerebral time variability is addressed by means of higher order derivative terms. In this sense, it represents an accurate noise template, specific to the SS record under investigation and largely independent from the additive measurement noise component. In fact, by construction $n_M[n]$ is statistically independent from $n_P[n]$, thus it does not belong to the vector subspace $\mathcal{T}$ and has

limited effect on the coefficient estimate (11).

Moreover, higher order expansion coefficients also have physical meaning and can be used as control variables in a closed-loop fashion. In particular, first derivatives of amplitude and phase are exploited to detect unexpected drifts or transients, which might reveal an acquisition system malfunction or an artifact due to subject movements. An SS record where the first-order term exceeds the threshold $|z_{(1,h)}|/|z_{(0,h)}| \geq 5\%$, $\forall h \in \mathcal{S}$, is considered unreliable and discarded from subsequent processing stages.

E. Subtraction and Average

The estimated noise template $\hat{n}_P[n]$ is finally subtracted from the corresponding LS record, yielding $\hat{r}[n]$. In accordance with the fNIRS model (1), it is reasonable to expect that physiological components are nearly eliminated, while the underlying HR is recovered to its original profile.

It is worth noticing that the noise template accounts only for physiological disturbances in a specific frequency range, neglecting random noise and physiological disturbances at different frequencies. As a matter of fact, narrow-band filtering, as discussed in Section III-B, should already have drastically reduced these effects.

Nonetheless, in practical applications this could be not enough. For this reason, data resulting from subtraction are slightly smoothed by means of a Savitski-Golay filter (with order equal to 3, length equal to 25 samples, as employed in CA).

After completion of the de-noising procedure, the recovered signal is segmented into trials and all those related to the same stimulus type are averaged to produce a mean HR estimate $\bar{h}_{HR}[n]$. A baseline correction is applied by subtracting the recovered signal mean value calculated in a time range of 1 s before the stimulus onset.

IV. DATA-SETS FOR METHOD ASSESSMENT

Both synthetic and real experimental data-sets have been employed to characterize the performances of the proposed algorithm and compare them with the reference techniques. Features of the data-sets are summarized in this Section.

A. Real data-set

Data were acquired at the Department of Developmental Psychology, University of Padova using a multi-channel, frequency domain NIR spectrometer (ISS Imagent^{TM}, Champaign, Illinois, USA) equipped with 32 laser diodes (16 emitting light at 690 nm and 16 at 830 nm) and 4 photo-multiplier tubes (PMT). Laser sources were modulated at 110 MHz, while the PMTs were modulated at 110.005 MHz, generating a 5.0 kHz heterodyning frequency. For each source-detector channel and wavelength the detected optical signal was converted into an AC output and further processed to recover HbO and HbR concentration changes. Sampling frequency was set to 7.8125 Hz. Sources and detectors were bilaterally placed on the motor cortex, as illustrated in Fig. 2, in order to obtain 5 LS channels and 2 SS channels per hemisphere.
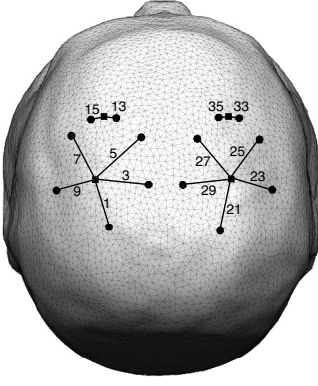
Fig. 2. Localization of acquisition channels for the experimental design. PMT locations are marked by squares, circles show the positions of laser diodes.

The experiment consisted in a finger-tapping task and was approved by the ethical committee of the University of Padova. Subjects were instructed to relax during the first part of the acquisition (resting state, RS) and were then presented with a random series of stimuli. Subjects' task was to perform a right (T1) or left (T2) hand finger tapping depending on the presented stimulus. For each condition (T1 or T2), 40 stimuli were presented, with an inter-stimulus interval ΔT ranging between 12 and 15 s.

B. Synthetic data-set

Let the experimental set-up provide a single stimulus at time index $n = 0$. The evoked response is then modelled by a linear combination of two time-variant gamma functions:

$$h_{HR}[n] = a \cdot (\Gamma_1[n, \tau_1, \sigma_1] - b \cdot \Gamma_2[n, \tau_2, \sigma_2]), \qquad (13)$$

where a defines the peak amplitude, b the undershoot level, τ_i and σ_i determine respectively the duration and the starting point of each gamma function, whose expression is:

$$\Gamma_i[n, \tau_i, \sigma_i] = \frac{1}{k!\tau_i} \left(\frac{n - \sigma_i}{\tau_i} \right)^k e^{-(n-\sigma_i)/\tau_i}. \qquad (14)$$

Scale factor k determines the actual responsiveness, in terms of peak latency and slope of the ascending edge.

Parameters in (14) have been suitably tuned to allow variations in HR peak amplitude[1] and latency among trials, within and between subjects. Their values are drawn from specific Gaussian distributions, whose means and standard deviations are reported in Table I. Inter-stimulus interval was set to $\Delta T = 12$ s.

The desired signal component $r[n]$ is a sequence of pulses, each having shape $h_{HR}[n]$, modulated by the revealing variable $\rho(k)$ which can assume either nil or unit value, depending on stimulus type (T1 or T2) and hemisphere location of the

---

[1]Amplitudes express molar concentration. Throughout the paper, values are reported in mol/dm^3 (also called "molar", symbol: M), as the unit traditionally used in the field, rather than in the SI unit mol/m^3. The conversion factor is: 1 M $= 10^3$ mol/m^3.

TABLE I.   HR AMPLITUDE AND LATENCY FOR T1 AND T2 RESPONSES

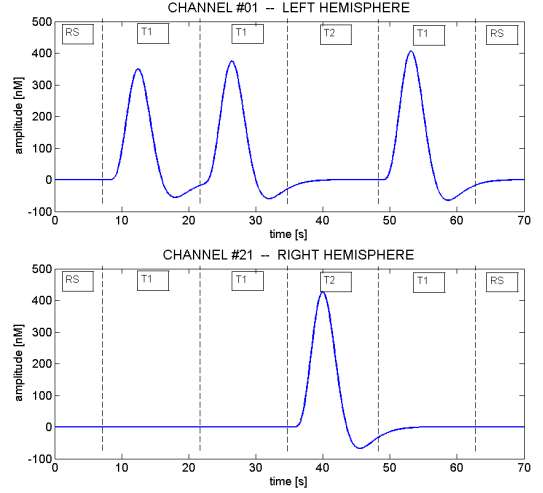|		Amplitude [nM]	Latency [s]
Right Hand T1	*mean*	360	5
	std dev	20	0.2
Left Hand T2	*mean*	420	5.5
	std dev	15	0.1

Fig. 3. HRs in two different channels (top: channel 1 – bottom: channel 21). Given the contralateral organization of the motor cortex, channels located in the left hemisphere refer to right-hand tapping (T1), while those located in the right hemisphere refer to left-hand tapping (T2).

selected channel:

$$r[n] = \sum_{i=1}^{N_{trials}} \rho[i] \cdot h_{HR}[n - i \cdot \Delta T] \qquad (15)$$

During resting states no event occurs in any LS channel.

Fig. 3 shows synthesized $r[n]$ signals for two channels, symmetrically located over the left and the right hemisphere. As expected, during RS periods both channels exhibit negligible contribution. Otherwise, HR responses are alternately shown by the two channels, respectively, during T1 and T2 events, reproducing a typical response to a finger tapping task consistent with the real experimental configuration.

To simulate a real scenario where each channel is measuring a different portion of the cortex, in some active channels the HR was added with halved amplitude.

Amplitudes and frequencies of the 5 physiological noise components simulating heart beat, respiration, vasomotion, slow and very slow physiological trends, are sampled from normal distributions whose means and standard deviations are reported in Table II, using the unit "molar" (symbol M) for molar concentration, whereas instantaneous phases ϕ_i belong to uniform distributions $\mathcal{U}(0, 2\pi)$. The reason for this variability is to simulate both differences among channels and non stationarity of physiological oscillations in the same

TABLE II.   MEAN +/- STD. DEV. OF PHYSIOLOGICAL COMPONENT
FREQUENCIES AND AMPLITUDES.

Component	Frequency [Hz]	Amplitude [nM]
Almost Stationary	$F_1 = .002 \pm .0001$	$A_1 = 700 \pm 100$
Ultra-low Freq.	$F_2 = .01 \pm .001$	$A_2 = 700 \pm 100$
Vasomotor	$F_3 = .07 \pm .04$	$A_3 = 400 \pm 10$
Respiratory	$F_4 = .2 \pm .03$	$A_4 = 200 \pm 10$
Cardiac	$F_5 = 1.1 \pm .1$	$A_5 = 400 \pm 10$

(a) Time Domain
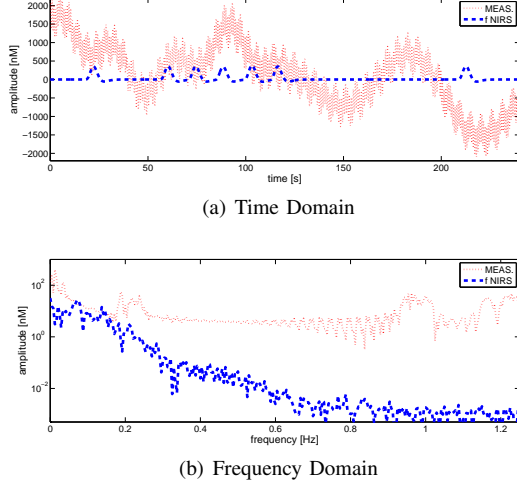

(b) Frequency Domain

Fig. 4.   Simulated LS signal (red) and a sequence of simulated HRs (blue).

channel.

Finally, random process $n_M[n]$ represents acquisition uncertainty as additive white Gaussian noise with mean value 400 nM and standard deviation 180 nM.

The relative proportion between the simulated HR profile $r[n]$ and the simulated noisy signal $x_{LS}[n]$ is presented in Fig. 4(a) for a 240 s observation interval. Underlying HRs are buried under low- and high-frequency oscillations, with the overall SNR being nearly -10 dB. The value is obtained from parameters in Table II estimated from real data. In the corresponding frequency domain plot of Fig. 4(b) HR spectra are entirely distorted by superposed physiological components.

V.   RESULTS

The proposed CS-TFM algorithm was implemented in the Matlab programming environment. Parameters for the CS stage were set-up to provide the necessary resolution in the frequency domain, record length being $N = 501$, whereas the super-resolution factor is $p = 11$, which yields $\Delta f_{CS} = 0.0014$ Hz. A second-order Taylor-Fourier expansion, i.e. $K = 2$, was selected as an optimal compromise between system redundancy and TFM de-noising capabilities.

Both synthetic and experimental data-sets refer to the same acquisition protocol. For every subject 14 channels are considered, 7 each for the right and left hemisphere, as presented in Fig. 2. An acquisition session lasts nearly 25 minutes and provides an alternate sequence of RS, T1 and T2 conditions.

HRs total 80 occurrences per channel, distributed between T1 and T2 responses on equal terms.

A. Synthetic Data-Sets

A synthetic data-set consists of 10 simulated subjects. By construction, underlying HRs are known a priori. For every channel, the CS-TFM average de-noised estimate $\bar{h}_{HR}[n]$ is computed from de-noised segments $\hat{h}_{HR}[n]$ according to the procedure in Sec. III-E. Given the nominal HR profile h^*_{HR}, response peak amplitude A^*_p and latency L^*_p, reconstruction accuracy is assessed by means of three quantitative indices:

$$
\begin{aligned}
RMS &= 100 \cdot \frac{\| h^*_{HR} - \bar{h}_{HR} \|}{\| h^*_{HR} \|} \\
AMP &= 100 \cdot \frac{|A^*_p - \bar{A}_p|}{|A^*_p|} \\
LAT &= |L^*_p - \bar{L}_p|
\end{aligned}
\tag{16}
$$

The first one determines the relative root-mean-square deviation between the nominal and recovered HR profile. The second considers the relative deviation of the response peak amplitude estimate, the third refers to latency.

Two operative conditions, with 10 simulated subjects each, are considered, called "ideal" and "realistic".

a) Ideal Data-Set: In the ideal condition, fNIRS measurement data are synthetically generated in accordance with model (1) provided in Section IV. For each channel, physiological noise components are generated as independent realizations of the same random variable. As a result, LS and SS contributions differ only partially and the SS channel subtraction approach is expected to drastically reduce physiological noise. In fact, the ideal data-set implements the assumption that informative and noisy contributions are statistically independent and uncorrelated.

Means and standard deviations of each index introduced in (16) are presented in Table III. Remarkably, none exceeds 1% relative error, showing that CS-TFM removes physiological oscillations almost entirely from LS sequences. Nominal and estimated HR profiles, presented in Fig. 5 for both full- and half-amplitude HRs, confirm that, in this ideal condition, the CS-TFM approach proves successful in removing noisy components from the informative ones.

b) Realistic Data-Set: In realistic conditions, a larger variability between LS and SS sequences is introduced. They are still generated independently, but from different random variables with specific and non coincident features. The assumption of uncorrelated additive noise is also weakened: LS and SS channels are located over different brain areas, their photons follow different paths. Hence, the noise template

TABLE III.   CS-TFM ACCURACY INDICES – HR RECONSTRUCTION
FROM SYNTHETIC IDEAL DATA-SET

	RMS [%]	AMP [%]	LAT [s]
mean	0.05	0.97	0.07
std dev	0.04	0.84	0.09

(a) Full Response

(b) Deviation from Reference
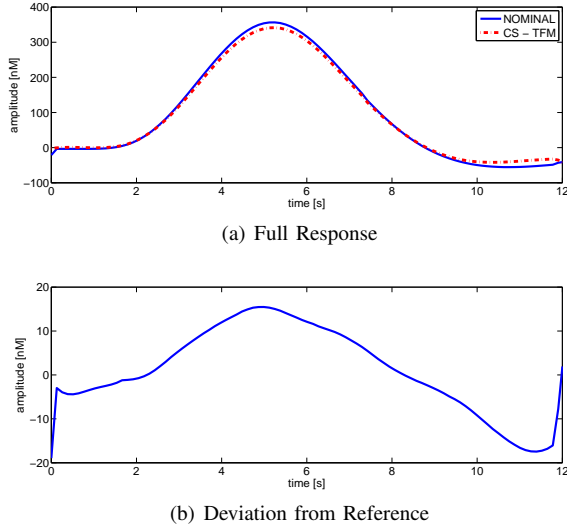
Fig. 5. Comparison between nominal (blue) and CS-TFM (red) response profiles in the ideal synthetic data-set.

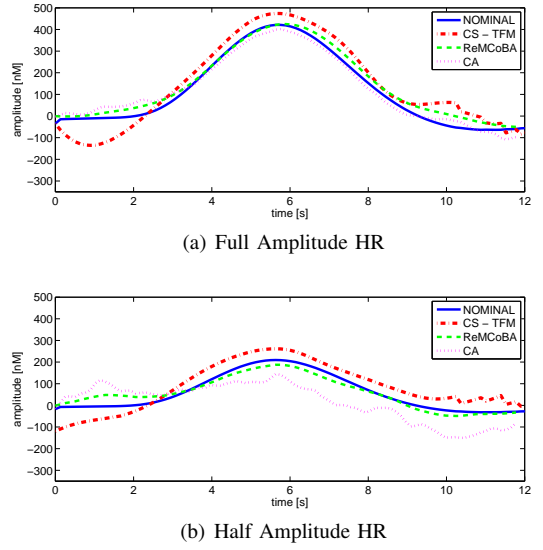(a) Full Amplitude HR

(b) Half Amplitude HR

Fig. 6. Comparison between nominal (blue) and CS-TFM (red), ReMCoBA (green), and CA (magenta) estimates of the HR profiles in the realistic synthetic data-set.
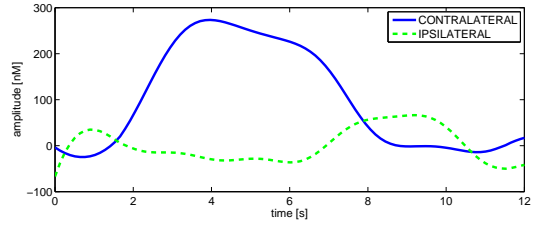
TABLE IV.   ACCURACY INDICES – HR RECONSTRUCTION FROM SYNTHETIC REALISTIC DATA-SET

		RMS [%]		AMP [%]		LAT [s]	
		Full	Half	Full	Half	Full	Half
CA	*mean*	23	120	23	53	0.43	0.89
	std dev	23	163	18	43	0.35	0.96
ReMCoBA	*mean*	9	47	12	27	0.38	0.78
	std dev	10.5	55	10	26	0.31	0.65
CS-TFM	*mean*	15	52	17	22.5	0.36	0.57
	std dev	7	12.6	8.2	8.3	0.32	0.42

Fig. 7. CS-TFM estimates of the HRs retrieved from a contralateral hemisphere channel (blue) and an ipsilateral hemisphere channel (green).

inferred from SS records may not represent exactly the oscillations measured in the LS records. Accordingly, it is reasonable to expect a degradation of algorithm performance compared to the "ideal" condition.

In this more challenging scenario, CS-TFM de-noised estimates have been compared with those provided by CA and ReMCoBA techniques. In Table IV, the corresponding accuracy indices are given in terms of mean and standard deviation, for both full- and half-amplitude HRs. Fig. 6 presents superposed CS-TFM, ReMCoBA and CA estimates, compared with the corresponding nominal profile.

CS-TFM reconstruction accuracy indices are noticeably worse than in the ideal condition, particularly, RMS error is significantly increased. As confirmed by Fig. 6, physiological oscillations partly survive the de-noising procedure and produce some distortion in the recovered response profile. However, this does not prevent reliable interpretation, as peak amplitude and latency deviations from the reference values are within about 20% and less than 1 s, respectively.

It is worth noting that CS-TFM outperforms CA in any considered configuration, as expected since CA does not use information coming from the SS signal. Conversely, ReM-

CoBA and CS-TFM estimates are close competitors. The former is better where RMS and AMP are considered, whereas the latter prevails in terms of LAT. CS-TFM also shows lower standard deviation, suggesting greater effectiveness in dealing with acquisition uncertainty.

B. Real Data-Set

The experimental data-set considered in this paper contains a single healthy participant acquisition, providing preliminary results on the applicability of the algorithm to data acquired in real settings. Due to the absence of a nominal reference HR profile, proper quantitative assessment of algorithm performance is almost unfeasible. However, based on prior functional investigations it is expected that a finger tapping task should produce larger HRs in the hemisphere contralateral to the hand used in tapping.

Results for the single acquired subject show this pattern of results. Fig. 7 considers two channels located over different hemispheres and confirms that in the contralateral one, a significant response is clearly detected, whereas in the ipsilateral one, only residual oscillations are apparent.

VI. Conclusion

A novel technique for fNIRS measurement data de-noising has been presented. The proposed CS-TFM algorithm is able to cope successfully with challenging conditions characterized by predominant non-stationary noisy contributions.

The acquired sample sequences are divided into reasonably short data records, which are processed singly, providing more accurate and specific subtraction templates. The algorithm relies on the SS channel paradigm, but a closed loop control based on noise component amplitude and phase derivatives allows a clear detection of motion artifacts or unexpected transients which could severely affect estimation accuracy.

Results considering both ideal and realistic synthetic data show a significant reduction of spurious components. These preliminary results are encouraging since the current performance of the algorithm is similar to that of ReMCoBA, an established fNIRS de-noising algorithm.

Future developments encompass the testing of the CS-TFM algorithm on a larger synthetic data-set (at least 30 simulated subjects) and on an experimental dataset composed of several participants, as well as trying to exploit the ability of the algorithm to work with fewer samples to recover single trials haemodynamic responses.

References

[1] S. Fazli, S. Dahne, W. Samek, F. Bieszmann, and K.-R. Muller, "Photonics technology for molecular imaging," *Proceedings of the IEEE*, vol. 103, no. 6, pp. 891–906, Jun 2015.

[2] M. Hosseini, B. Araabi, and H. Soltanian-Zadeh, "Pigment melanin: Pattern for iris recognition," *Instrumentation and Measurement, IEEE Transactions on*, vol. 59, no. 4, pp. 792–804, Apr 2010.

[3] M. Larrain, A. Guesalaga, and E. Agosin, "A multipurpose portable instrument for determining ripeness in wine grapes using NIR spectroscopy," *Instrumentation and Measurement, IEEE Transactions on*, vol. 57, no. 2, pp. 294–302, Feb 2008.

[4] J. Leis, D. Buttsworth, C. Snook, and G. Holmes, "Detection of potentially explosive methane levels using a solid-state infrared source," *Instrumentation and Measurement, IEEE Transactions on*, vol. 63, no. 12, pp. 3088 – 3095, Dec 2014.

[5] G. Salvatori, K. L. Suh, R. R. Ansari, and L. Rovati, "Instrumentation and calibration protocol for a continuous wave near infrared hemoximeter," *Instrumentation and Measurement, IEEE Transactions on*, vol. 55, no. 4, pp. 1368–1376, Aug 2006.

[6] Y. Yamakoshi, M. Ogawa, T. Yamakoshi, M. Satoh, M. Nogawa, S. Tanaka, T. Tamura, P. Rolfe, and K. Yamakoshi, "A new non-invasive method for measuring blood glucose using instantaneous differential near infrared spectrophotometry," in *Engineering in Medicine and Biology Society, 2007. EMBS 2007. 29th Annual International Conference of the IEEE*, Aug 2007, pp. 2964–2967.

[7] M. Arnold, J. Olesberg, and G. Small, *Near-Infrared Spectroscopy for Noninvasive Glucose Sensing*. Wiley, 2010, ch. 13.

[8] D. A. Boas, C. E. Elwell, M. Ferrari, and G. Taga, "Twenty years of functional near-infrared spectroscopy: introduction for the special issue." *NeuroImage*, vol. 85 Pt 1, pp. 1–5, 2014.

[9] F. F. Jöbsis, "Noninvasive, infrared monitoring of cerebral and myocardial oxygen sufficiency and circulatory parameters." *Science*, vol. 198, no. 4323, pp. 1264–7, 1977.

[10] R. B. Buxton, *Introduction Functional Magnetic Resonance Imaging Principles And Techniques*. Cambridge University Press, 2002.

[11] E. Kirilina, A. Jelzow, A. Heine, M. Niessing, H. Wabnitz, R. Brühl, B. Ittermann, A. M. Jacobs, and I. Tachtsidis, "The physiological origin of task-evoked systemic artefacts in functional near infrared spectroscopy." *NeuroImage*, vol. 61, no. 1, pp. 70–81, 2012.

[12] B. Widrow, J. Glover, J.R., J. McCool, J. Kaunitz, C. Williams, R. Hearn, J. Zeidler, J. Eugene Dong, and R. Goodlin, "Adaptive noise cancelling: Principles and applications," *Proceedings of the IEEE*, vol. 63, no. 12, pp. 1692 – 1716, Dec 1975.

[13] Y. Kadah, "Adaptive denoising of event-related functional magnetic resonance imaging data using spectral subtraction," *Biomedical Engineering, IEEE Transactions on*, vol. 51, no. 11, pp. 1944 – 1953, Nov 2004.

[14] P. Allen, J. O., and R. Turner, "A method for removing imaging artifact from continuous EEG recorded during functional MRI," *Neuroimage*, vol. 12, pp. 230–239, 2000.

[15] M. Bertocco, G. Frigo, and C. Narduzzi, "On compressed sensing and superresolution in DFT-based spectral analysis," in *Proc. of 17th IMEKO International Workshop on ADC Modelling and Testing*, July 18-19, 2013, pp. 615–620. [Online]. Available: http://www.imeko.org/publications/tc4-2013/IMEKO-TC4-2013-170.pdf

[16] G. Frigo and C. Narduzzi, "EEG gradient artifact removal by compressive sensing and Taylor-Fourier transform," in *Medical Measurements and Applications (MeMeA), 2014 IEEE International Symposium on*, June 2014, pp. 1–6.

[17] G. Frigo, S. Brigadoi, G. Giorgi, G. Sparacino, and C. Narduzzi, "A compressive sensing spectral model for fNIRS haemodynamic response de-noising," in *Medical Measurements and Applications (MeMeA), 2015 IEEE International Symposium on*, May 2015, pp. 244–249.

[18] R. Saager and A. Berger, "Measurement of layer-like hemodynamic trends in scalp and cortex: implications for physiological baseline suppression in functional near-infrared spectroscopy." *Journal of biomedical optics*, vol. 13, no. 3, p. 034017, 2008.

[19] L. Gagnon, K. Perdue, D. N. Greve, D. Goldenholz, G. Kaskhedikar, and D. A. Boas, "Improved recovery of the hemodynamic response in diffuse optical imaging using short optode separations and state-space modeling," *NeuroImage*, vol. 56, no. 3, pp. 1362 – 1371, 2011.

[20] M. Calderon-Arnulphi, A. Alaraj, and K. V. Slavin, "Near infrared technology in neuroscience: past, present and future." *Neurological research*, vol. 31, no. 6, pp. 605–14, 2009.

[21] R. B. Saager and A. J. Berger, "Direct characterization and removal of interfering absorption trends in two-layer turbid media," *Journal of the Optical Society of America A*, vol. 22, no. 9, p. 1874, 2005.

[22] F. Scarpa, S. Cutini, P. Scatturin, R. Dell'Acqua, and G. Sparacino, "Bayesian filtering of human brain hemodynamic activity elicited by visual short-term maintenance recorded through functional near-infrared spectroscopy (fNIRS)," *Opt. Express*, vol. 18, no. 25, pp. 26 550–26 568, Dec 2010. [Online]. Available: http://www.opticsexpress.org/abstract.cfm?URI=oe-18-25-26550

[23] F. Scarpa, S. Brigadoi, S. Cutini, P. Scatturin, M. Zorzi, R. Dell'Acqua, and G. Sparacino, "A reference-channel based methodology to improve estimation of event-related hemodynamic response from fNIRS measurements," *NeuroImage*, vol. 72, no. 0, pp. 106 – 119, 2013.

[24] G. Frigo and C. Narduzzi, "Compressive sensing with an overcomplete dictionary for high-resolution dft analysis," in *Signal Processing Conference (EUSIPCO), 2014 Proceedings of the 22nd European*, Sept 2014, pp. 1766–1770.

[25] J. Tropp and A. Gilbert, "Signal recovery from random measurements via orthogonal matching pursuit," *Information Theory, IEEE Transactions on*, vol. 53, no. 12, pp. 4655–4666, Dec 2007.

[26] M. A. Platas-Garza and J. A. de la O Serna, "Dynamic phasor and frequency estimates through maximally flat differentiators," *IEEE Trans. Instrum. Meas.*, vol. 59, no. 7, pp. 1803–1811, Jul. 2010.